PAPER

Femtosecond photonic viral inactivation probed using solid-state nanopores

To cite this article: Mina Nazari *et al* 2018 *Nano Futures* **2** 045005

NANO FUTURES

PAPER

Femtosecond photonic viral inactivation probed using solid-state nanopores

Mina Nazari[1,2], Xiaoqing Li[3], Mohammad Amin Alibakhshi[4], Haojie Yang[5], Kathleen Souza[6], Christopher Gillespie[6,11], Suryaram Gummuluru[7], Mi K Hong[8], Björn M Reinhard[2,9], Kirill S Korolev[8,10], Lawrence D Ziegler[2,9], Qing Zhao[3], Meni Wanunu[4,12] and Shyamsunder Erramilli[2,8,12]

[1] Department of Electrical and Computer Engineering, Boston University, Boston, MA 02115, United States of America
[2] Photonics Center, Boston University, Boston, MA 02115, United States of America
[3] School of Physics, Peking University, Beijing, People's Republic of China
[4] Department of Physics, Northeastern University, Boston, MA 02115, United States of America
[5] Department of Mechanics, Southeast University, Nanjing, People's Republic of China
[6] Next Generation Bioprocessing, MilliporeSigma, Bedford, MA 01730, United States of America
[7] Department of Microbiology, Boston University School of Medicine, Boston, MA 02118, United States of America
[8] Department of Physics, Boston University, Boston, MA 02115, United States of America
[9] Department of Chemistry, Boston University, Boston, MA 02115, United States of America
[10] Department of Bioinformatics Program, Boston University, Boston, MA 02115, United States of America
[11] Current address of C Gillespie: Immunogen, 830 Winter St Waltham MA, United States of America.
[12] Authors to whom any correspondence should be addressed.

E-mail: wanunu@neu.edu **and** shyam@bu.edu

Keywords: nanopore, virus, plasmon, femtosecond, laser

Supplementary material for this article is available online

RECEIVED
21 August 2018

ACCEPTED FOR PUBLICATION
7 September 2018

PUBLISHED
24 September 2018

Abstract

We report on detection of virus inactivation using femtosecond laser radiation by measuring the conductance of a solid state nanopore designed for detecting single particles. Conventional methods of assaying for viral inactivation based on plaque forming assays require 24–48 h for bacterial growth. Nanopore conductance measurements provide information on morphological changes at a single virion level. We show that analysis of a time series of nanopore conductance can quantify the detection of inactivation, requiring only a few minutes from collection to analysis. Morphological changes were verified by dynamic light scattering. Statistical analysis maximizing the information entropy provides a measure of the log reduction value. This work provides a rapid method for assaying viral inactivation with femtosecond lasers using solid-state nanopores.

1. Introduction

Existing and emerging viruses are a major threat to human and veterinary public health. The need for safe and reliable inactivation or removal of viruses is universal in antiviral therapies, pharmaceuticals, and viral vaccine development. Conventional pharmaceutical pathogen inactivation methods are quite effective, but they involve substantial collateral damage and have undesirable side-effects [1–3]. Chemical-free viral inactivation methods such as ultraviolet and gamma-irradiation have been used to minimize some of the side-effects. Nevertheless, these methods adversely affect thermolabile compounds and denature biomolecules of interest in the medium containing the virus. Ultrashort pulsed lasers (UPL) provide new opportunities for chemical-free pathogen disinfection in solution. Photonic methods have the potential to provide an attractive alternative to existing biocides and ionizing radiation techniques [4–8]. Photonic inactivation has been successfully achieved with focused femtosecond (fs) laser pulses for exposure times of $\geqslant$1 h on sample volumes typically of $\leqslant$2 ml [5–10]. Although the ultrafast laser inactivation method for viral inactivation is fairly well established, a systematic understanding of the inactivation mechanism is currently lacking. There is a need for rapid methods for assaying viral inactivation in order to carry out multi-dimensional studies of the ultrafast laser parameters such as

intensity, pulse duration and center wavelength that can contribute to the design and optimization of inactivation protocols.

Viral inactivation is a complicated process and its outcome highly depends on the specific treatment method. A wide range of biological assays could detect and quantify intact viruses in an ensemble manner which is extremely laborious, time-consuming, with low sensitity [11]. A different approach is to explore viruses at the single virion level. Different optical methods have been developed to characterize single viral particles; [12–14] but still there is a need for a technique that is fast, sensitive and uses small sample volumes. Although imaging techniques, such as AFM and TEM, are capable of characterizing viruses with high sensitivity, results will be inevitably affected by the tedious and costly sample preparation steps. Nanometer-sized pores in a membrane offer the capability of electrically detecting molecules in a label-free manner at single-molecule level in a volume as small as a few microliters and detection times as short as a few seconds. Passage of molecules and particles through a nanopore causes transient disruption in the ionic current through it, from which the size, concentration, and distribution of analytes can be deduced [15, 16]. The electrical signal characteristics in a given analyte sample strongly depend on the analyte passing through the pore, the pore geometry, and the experimental conditions such as pH, ionic strength, applied voltage, temperature, etc. This single-particle electrical sensor has been used for quantifying the conformational properties of proteins [17–23], understanding DNA transport [24–26] and detecting small molecules [27, 28], among many other applications. Previous studies have reported the ability of nanopore sensors to detect spherical and icosahedral viruses [29], virus capsids [30], the masses and zeta potentials of viruses [31, 32], and to explore the translocation of stiff, rod-shaped viruses [33].

This ability of nanopores to detect the translocation of nanometer size particles motivated us to study the effect of an optical viral therapy on the single virus level, crucial for the preparation of very safe biotherapeutics. In this paper, high incident fs laser pulse intensities of >100 GW cm^{-2}, which are more than 10^5 times greater than used in previous studies, have been used to inactivate viruses, leading to 4-log reduction in viral activity in 1 min irradiation of $\sim$2 ml sample volume. This result shows nearly more than two orders of magnitude improvement in treatment time compared to conventional pulsed laser viral inactivation methods [34]. Furthermore, we demonstrate the capability of the nanopore technique to precisely characterize individual viruses, explore how vital viral function is affected by treatment, and quantify the effectiveness of this label-free viral inactivation technique. In light of these points, we investigate the effects of fs laser on inactivated ΦX174 bacteriophage, which has the first sequenced DNA-based phage genome widely used standard for viral clearance, as well as a surrogate for enteric human viruses [35]. Changes in the physical properties of treated virus samples are monitored by electrically counting viruses in a small sample volume. A statistics-based method has been developed to monitor the reduction value of viruses using sequential nanopore measurements, and compared with a plaque forming assay. Moreover, the effect of inactivation on viruses in an ensemble manner and at the single-virus level resulting from dynamic light scattering (DLS) measurements and nanopores, respectively, are compared.

2. Methods

2.1. Femtosecond laser irradiation

Femtosecond laser pulses from a Legend Elite Duo (Coherent Inc.) A Ti-sapphire regenerative amplifier system was used as the excitation source in this study. This laser produces a continuous train of 35 fs pulses at a repetition rate of 1 kHz. The output of the second harmonic generated by a ~ 1mm thick BBO crystal with a wavelength centered at $\sim$400 nm was used to irradiate the virus samples, with a combined pulse energy of the second harmonic and fundamental of about 2.5 mJ. Figure 1(a) depicts the experimental setup. The laser beam with spot size $\sim$1 cm^2 was incident upon a typically 1 cm quartz cuvette containing 2 ml of virus sample while a stirrer was used to homogenize the virus's interaction with the laser beam. For ΦX174 sample with 10^{12} pfu ml^{-1} concentration, the laser treatment is made by exposing 250 μl of viruses in 2 mm cuvette. The typical sample exposure time was 15 minutes. All experiments were carried out at 22 °C, and all samples were immediately stored at 4 °C after irradiation. Experiments were carried out in triplicate.

2.2. Virus sample preparation

ΦX174 samples with 2×10^{12} plaque forming unit (pfu) per ml concentration (Promega TiterMax ΦX174 Bacteriophage) in 0.05 M sodium tetraborate were stored at -80 °C. Before the experiment, samples were thawed to room temperature, aliquoted, and kept at 4 °C. For diluted samples, ΦX174 spiked feed solutions were prepared by serial dilution in Sorenson's buffer to the final concentration of approximately 10^6 pfu ml^{-1}.

2.3. Infectious plaque assay

To count the ΦX174 in the solution, samples were diluted with Sorensen's buffer dilution blanks, to bring plaque to within a statistically valid range of 30–300 plaques per plate. Samples were assayed in triplicate by adding

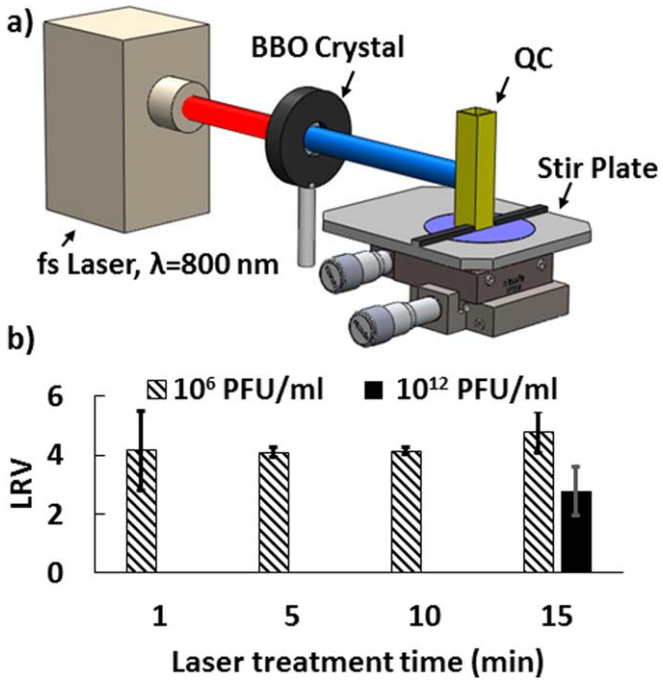

Figure 1. (a) Schematic of experimental setup for photonic viral inactivation. The following abbreviation are used: fs: femtosecond, QC: quartz cuvette, BBO: Beta barium borate. (b) Log reduction value (LRV) measured for ΦX174 virus with 10^6 pfu ml^{-1} (patterned) and six-orders of magnitude increased concentration (solid) after USP laser irradiation for different exposure time.

0.1 ml of diluted sample and 0.1 ml of host cell suspension to a test tube containing 3 ml of molten (46 °C–48 °C) ΦX174 overlay agar consist of 10 g of tryptone peptone (Difco), 8.5 g of agar (Difco) and 5 g of NaCl per liter of reagent water. Then the solution containing host cell and bacteriophage was vortexed and transferred to the ΦX174 bottom plate agar (2.5 g of NaCl, 2.5 g of KCl, 10 g of tryptone peptone from Difco, 10 g of agar from Difco, and 1 ml of 1 M $CaCl_2$ per liter of reagent grade water) and incubated overnight at 37 °C. Then plaques were counted and the corresponding bacteriophage concentrations were reported as pfu mL^{-1}. Sorensen's phosphate buffer (pH 7.3), ΦX174 bottom plate agar, and ΦX174 overlay agar were purchased from Northeast Laboratory Services (Winslow, ME).

2.4. Nanopore device fabrication and measurement

Our electrical detection system is composed of a nanopore formed in a 50 nm-thick insulating silicon nitride (SiN) membrane. The SiN is deposited on a silicon substrate with 2 micron silicon dioxide previously grown on, which is chemically etched by potassium hydroxide (KOH) to obtain a freestanding membrane. The electron beam of a JEOL 2010F transmission electron microscope (TEM) was finely focused on the membrane in order to make a pore with controlled size [24]. The choice of 38 nm nominal diameter of the nanopore was based on the known radius of the virus derived from its x-ray structure. Several slightly smaller and larger nanopores were tested to obtain the optimal pore size. A more detailed systematic study was not attempted. The as-fabricated nanopore chip is then mounted in a fluoropolymer cell that allows electrical measurement of ionic current through the nanopore. The cell is filled with 0.1 M KCl solution (16.1 mS cm^{-1} conductivity), buffered to pH 7 using 10 mM tris. The silver–silver chloride (Ag/AgCl) electrodes are inserted in both cis- and trans-chambers, and a DC voltage is applied to flow current and drive charged molecules through the pore.

2.5. Data acquisition and analysis

A Chimera VC100 (Chimera Instruments LLC) was used for recording the ion current through the nanopore. Data was digitized at 4.17 MS s^{-1}, and saved to the computer at a 1 MHz bandwidth. Prior to analysis, recordings were further filtered using a 100 kHz digital low-pass filter. To verify the pore's stability, before the introduction of a virus sample to the nanopore, several seconds of current were collected to ensure that no event is detected and the baseline current is stable. Three key independent parameters are extracted from the nanopore data: the dwell time of viruses at the pore, t_d, the fractional current blockade, F_I, and the inter-event waiting time, δt, from which virus capture rates can be extracted.

2.6. Dynamic light scattering (DLS)

In order to obtain information on the size distribution of viruses in an ensemble manner, we performed DLS measurements using the Zetasizer Nano S90 from Malvern Corp. This DLS measurement is based on the Brownian motion of spherical particles; using the Stokes–Einstein relation to determine the particle size based on measured diffusion constant of particles [36]. For the size measurement, ΦX174 virus with 10^{12} pfu ml^{-1} concentration and ΦX174 Virion DNA (New England Biolabs) with 1000 μg ml^{-1} concentration, are diluted by 8-fold and 30-fold respectively in 10 mM Tris. An aliquot of about 80 μl of the diluted samples is transferred to the cuvette for DLS analysis with the measurements performed at 23 °C.

3. Results and discussion

Obtaining extremely high levels of viral clearance is a substantial step in the purification of protein-based therapeutics. The presence of even a single virus in the final drug product could be harmful to the consumer's health. To prevent this, implementation of an effective viral inactivation strategy is crucial. USP viral inactivation with greater than 4-log reduction in viral infectivity would enable a new chemical-free pathogen clearance technology [34, 37, 38]. The first objective of this study is to extend the work done on USP inactivation of viruses, using a regeneratively amplified laser system. We expedite the reported USP photonic inactivation (>1 h) [34] to 1 min. In this study, 35 femtosecond pulsed laser irradiation working at ~400 nm is used to irradiate 2 ml of ΦX174 bacteriophage for different irradiation times. Inactivation of viruses is measured by a viral infectivity assay. Original sample concentrations were calculated by multiplying the plate count by the dilution factor, reported as pfu ml^{-1} [39].

The final results for the viral inactivation experiments is reported as the log reduction value (LRV) which provides a direct measure of viral inactivation. The LRV was calculated according to:

$$\mathrm{LRV} = \log_{10}\left(\frac{C_U}{C_T}\right). \tag{1}$$

Here C_U is the concentration of the untreated sample and C_T the concentration of the treated samples exposed to the laser irradiation as described. Control samples consist of a sample with no laser exposure which was kept refrigerated during the experiment and another sample which experienced the same pipetting and stirring condition as treated sample but without the laser exposure. These control samples never differed significantly and were taken to check for loss of titer in the treated suspension. As demonstrated in figure 1(b) more than 10^4 reduction values of ΦX174 with 10^6 pfu ml^{-1} concentration is achieved by irradiating 2 ml of virus suspension with 2.5 W (average power) ~ 400 nm femtosecond laser pulses for different treatment times ranging from 1 to 15 min. The relatively large laser beam diameter of the regeneratively amplified laser beam results in fast viral treatment which can overcome the need for long irradiation times, and remove constraints on the corresponding practical implementation.

The next goal is to precisely monitor changes occurred to the treated viruses on the single virus level. A 20 μl aliquot of ΦX174 with ~10^{12} pfu ml^{-1} is treated for 15 min exposure with the same laser setup. For this low volume of sample, we used a micro quartz cuvette with no stirring. Again, the strong reduction in viral infectivity (LRV $>$ 3) was achieved for six-orders of magnitude increased virus concentration (figure 1(b)).

As shown in figure 2, the ΦX174 viruses are being voltage-driven through a ~38 nm pores made of SiN. A TEM image of the pore is shown as an inset. The pore size is intentionally chosen close to the virus size to slow down the translocations and allow for accurate measurement of the events. Viruses are electro-osmotically driven through the nanopores upon application of a negative bias to the trans chamber. The application of voltage results in a steady-state countercurrent of K^+ and Cl^- ions across the pore, which produces a stable baseline open pore current, I_0. When 0.5 μl of virus sample is added to 50 μl of buffer in the cis chamber, passage of individual viruses through the pore reduces the ionic current, which results in a spike in the measured current. This volume was sufficient to generate $>2 \times 10^3$ events in 10 s for good statistics in the untreated sample. The spike contains information about single virions, which can be extracted using statistical analysis methods. The current is measured by a Chimera VC100 amplifier which streams 1 MHz bandwidth data to a computer at a sampling rate of 4.17 MHz, followed by application of a 100 kHz low-pass filter in software to reduce the high frequency noise dominated by the chip capacitance. The choice of the 100 kHz low-pass filter reflects a compromise that enables detection of events with a sufficient sampling time-resolution of one order of magnitude smaller than the virus translocation times, and the loss of higher frequency information.

Figure 3(a) shows continuous current traces obtained when untreated ΦX174 viruses were added to the cis chamber at 40 mV applied voltage. Each spike corresponds to transport of a single virus through the ~38 nm pore. The electric signal represents two predominant current levels, the higher one corresponds to the open pore current

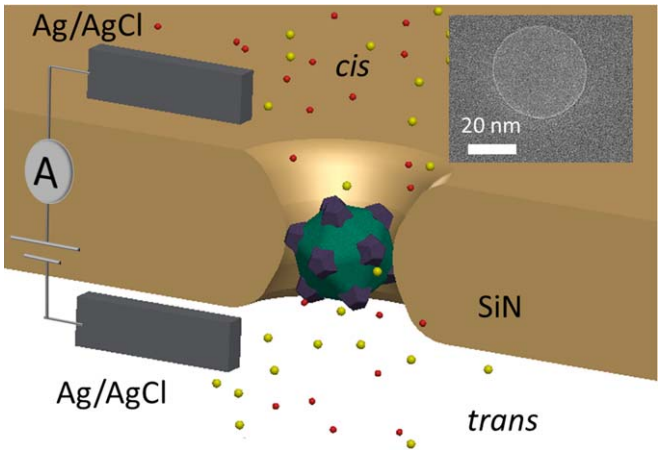

Figure 2. Schematic of the nanopore setup for virus detection. Pores are fabricated in freestanding SiN membranes and an external bias is applied across the membrane to drive ΦX174 viruses, potassium ions (yellow dots) and chloride (red dots) ions through the pore. Inset: TEM image of a fabricated nanopore. (scale bar: 20 nm).

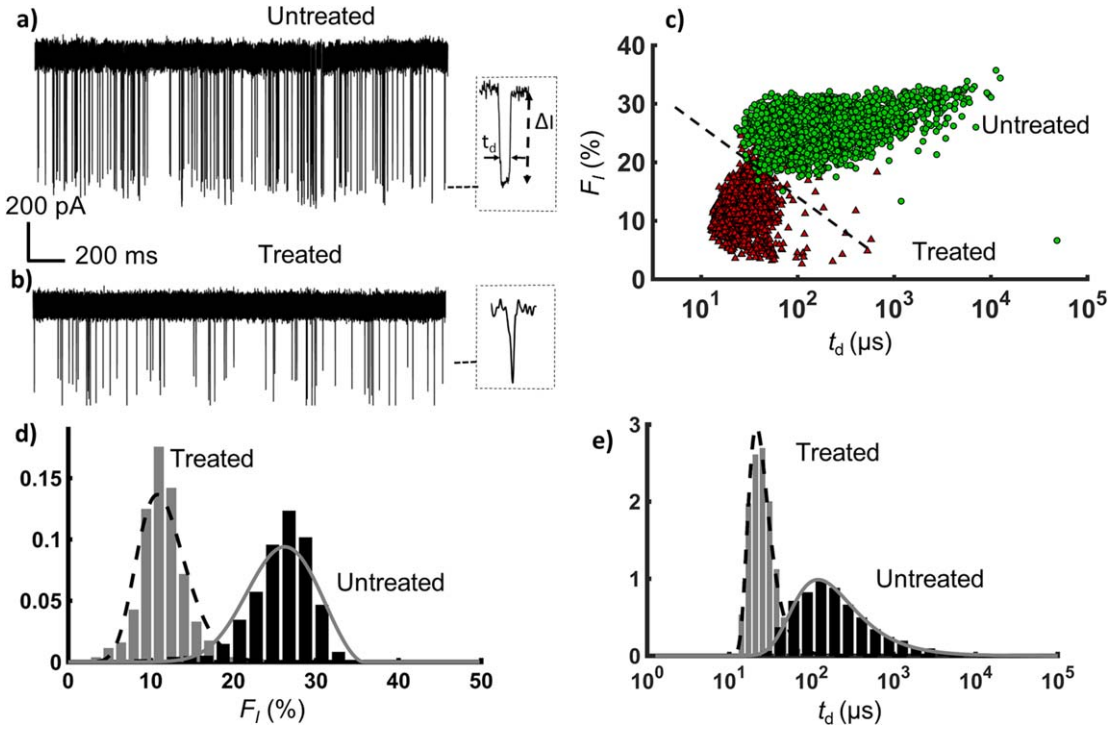

Figure 3. Comparison of pre-treatment and post-treatment of ΦX174 virus with a pulsed (35 fs) 800 and 400 nm laser with an average power of 2.5 W for 15 min. (a), (b) Continuous ionic current traces collected using a 40 mV applied voltage, low-pass filtered to 100 kHz. Inset: zoomed in portion of selected representative events. (c) Scatter plot of fractional current blockade, F_I (%), at 40 mV (0.1 M KCl, 20 °C) vs dwell time, t_d. (d) Histograms of fractional current blockade at 40 mV showing decrease after laser treatment. (e) Histograms of dwell time at 40 mV voltage demonstrates faster translocation of treated viruses.

when viruses do not translocate through the pore, I_0, and the lower corresponds to the virus-occupied level. Based on the measured open pore current which is 1.13 nA, the pore conductance was calculated as $G = 28.2$ nS. The inset shows a magnified view of a randomly selected event corresponding to individual intact ΦX174. The translocation current, ΔI, which is the difference between the baseline current and the pulse minimum, depends on pore geometry and virus size. Based on the known nanopore diameter of ~ 38 nm, the nanopore length was estimated from the open pore conductance to be $h_{eff} \sim 35$ nm. This value, thinner than the overall initial 50 nm membrane thickness, h, was still thicker than the expected thickness of $h_{eff} = h/3$ previously found for the very narrow pores [40]. As shown in figure 3(d), the mean fractional current blockade for untreated ΦX174 virus is measured to be 27%. This number is consistent with the 29% blockade predicted by the following theoretical equation, derived in supplemental material is available online at stacks.iop.org/NANOF/2/045005/mmedia,

for a 30 nm diameter spherical virus:

$$F_I = \frac{\langle \Delta I \rangle}{I_o} = \frac{R_b - R_o}{R_b}. \tag{2a}$$

In which $R_o = \frac{1}{\sigma d_p} + 4\frac{h_{eff}}{\sigma \pi d_p^2}$ is the open pore resistance and R_b is the nanopore resistance in the blocked state:

$$R_b = \frac{1}{\sigma d_p} + 4\frac{h_{eff} - d}{\sigma \pi d_p^2} + \frac{4}{\sigma \pi \sqrt{d_p^2 - d^2}} \tan^{-1}\left(\frac{d}{\sqrt{d_p^2 - d^2}}\right) \quad (h_{eff} \geqslant d). \tag{2b}$$

Here d is the virus diameter, d_p is the pore diameter, and σ is the salt conductivity which for the 100 mM KCl buffer was measured as 16.7 mS cm^{-1} using the conductivity meter.

The agreement between theoretical and experimental translocation ratio verifies that the untreated viruses maintain their shape integrity during transport through the pore. Additionally, a 1D drift–diffusion model can be used to describe the dwell time distribution of virus translocation through the nanopores. Fitting the probability density function of dwell time distribution (t_d) with the following equation yields two important parameters: diffusion constant of viruses inside the nanopore, D_{pore}, and their drift velocity, v_d

$$P(t) = \frac{h_{eff}}{\sqrt{4\pi D_{pore} t_d^3}} \exp\left(\frac{-(h_{eff} - v_d t_d)^2}{4 t_d D_{pore}}\right). \tag{3}$$

Application of this equation, which is based on the assumption of barrier-free transport [41], for the untreated viruses (figure 3(e)) yields $D_{pore} = 0.5\ \mu\text{m}^2\ \text{s}^{-1}$ and $v_d < 10^{-4}$ m s^{-1}.

To gain insight into the virus transport kinetics through this nanopore, we compare the in-pore diffusion coefficient of viruses with a bulk diffusion coefficient, using Stokes−Einstein equation $D = \frac{k_B T}{3\pi\eta d}$ where k_B is the Boltzmann constant, T the absolute temperature, η the viscosity of the solution, and d the hydrodynamic diameter of the virion. Using DLS we measured average diameters of ~30 nm at 23 °C, and accordingly, D_{bulk} was calculated as 14 $\mu\text{m}^2\ \text{s}^{-1}$. The result shows a small reduction in D_{pore} which can be a consequence of virus-pore hydrodynamic interaction, as previously observed with protein transport through smaller pores [42].

Upon successful detection of untreated viruses using nanopores, we probed the effect of laser treatment on the virus sample. A time trace for translocation of laser-treated ΦX174 with LRV $>$ 3 (figure 1(b)) is shown in figure 3(b). There is a drastic change in the time trace of laser irradiated viruses as compared to untreated samples which will be explored in more detail. The averaged baseline conductance remained constant to within 1% over the data collection timescale, indicating that the nanopores did not expand and were not blocked by debris or other particles.

To explore the effect of laser treatment, the scatter plot of fractional current blockade versus dwell time of treated and untreated viruses at 40 mV voltage is shown in figure 3(c). Two clear groupings of events are visibly noted, corresponding to the treated and untreated viruses which can be visually distinguished by drawing a line as shown in figure 3(c). A histogram of fractional current blockades and dwell time distributions for both treated and untreated samples at 40 mV along with generalized extreme value distribution fits to the distributions are shown in figures 3(d)–(e) respectively. The untreated sample is centered at $F_I = 25.04+/-3.1\%$ with $\log_{10}(t_\text{d}) = 2.05+/-0.36$ (t_d measured in μs) and the treated sample is centered at $F_I = 10.4+/-2.7\%$ with $\log_{10}(t_\text{d}) = 1.3+/-0.12$. These two sets of independent parameters (F_I and t_d) clearly show the effect of laser treatment on viruses. The F_I is related to the size of the particle and hence a strong decrease in the fractional blockade yields the first important information on the effect of fs laser treatment, i.e., the global appearance of the non-enveloped ΦX174 virus does not remains intact after treatment which is in agreement with previously established data [8]. Measurements of the fractional blockade with slightly larger diameter nanopores ($d_p \sim$ 39–40 nm) gave results similar to those reported in figure 3 whereas a smaller diameter nanopore produced events with longer dwell times. A systematic study of the pore size dependence on treated and untreated samples was not attempted, given the limited scope of the present study.

Using the capability of our label-free resistive pulse technique, one can monitor the inactivation of viruses by looking for the presence of intact viruses in the solution with high sensitivity. One simple model is to consider an ellipse in the scatter plot of untreated events centered at the mean value of fractional current in y direction and the mean of $\log_{10}(t_\text{d})$ in x direction. The semi-minor and semi-major axis radius of this ellipse is equal to three times the standard deviation of the F_I and $\log_{10}(t_\text{d})$ of untreated events, respectively (figure 4(a)). The standard deviations are obtained based on the Gaussian fits of the corresponding data. Counting the number of the treated (red) data points in the black ellipse gives us a rough estimate of the number of intact viruses in the treated sample, n. The number of points in untreated and treated scatter plot is 2723 and 2564, respectively. The

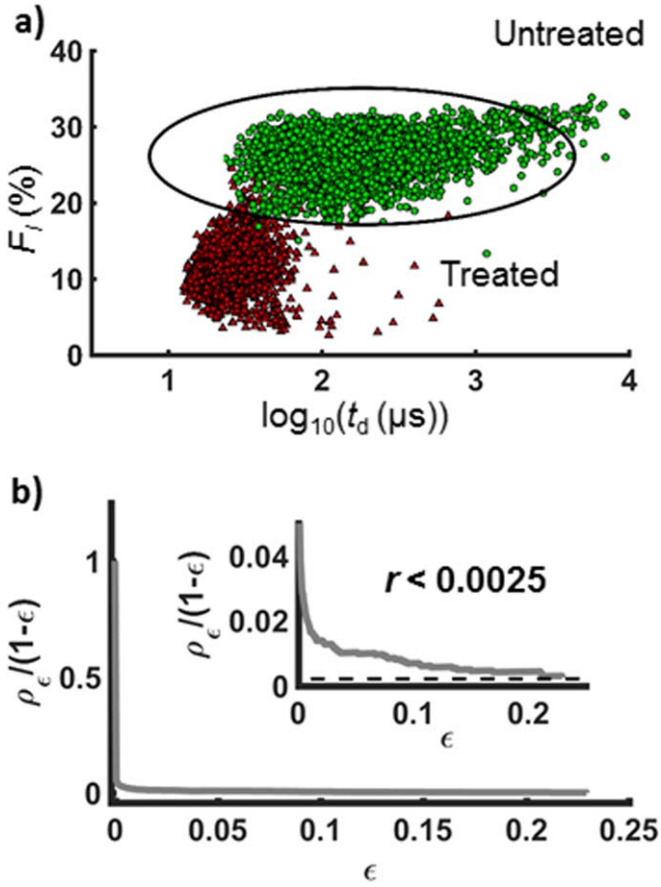

Figure 4. (a) Scatter plot of fractional blockade of untreated (green) and treated (red) viruses versus event duration, under a driving voltage of 40 mV (b) upper bound determination of the survival fraction, inset shows the zoom in plot of the graph. The minimum occurs at $\varepsilon = 0.2294$.

ratio of n to the total number of red data points of the treated sample, N, gives us an estimation of the survival fraction (r)

$$r = \frac{f_I}{f_T}\frac{n}{N}, \tag{4}$$

where f_I and f_T are the capture probabilities of intact and treated virus. Assuming these probabilities to be equal in this case, the survival fraction is approximately 0.02. This quantity can provide a simple method for rapidly estimating the efficiency of the inactivation technique.

A more precise way to estimate r using nanopore data is to determine an upper bound for the number of survived viruses after treatment. To find the upper bound we developed a statistical formula that employs a probability distribution function derived from figure 3(d). The first step is to estimate the probability of finding a translocation event of the treated sample with a distinguishing feature x_T inside the untreated sample region with x_U. In a simplest case x_T and x_U can be any feature that can separate the two populations; in our case it can be fractional current blockade, dwell time or any other combination of these two. For example if we consider this one dimensional scalar as the fractional current blockade, in our case there is a big separation between the mean of untreated events, $\overline{x_U}$, and treated ones, $\overline{x_T}$, so that $\overline{x_T} < \overline{x_U}$. Some of the viruses in the treated sample could be intact. We can quantify this possibility by considering the probability $P_I(x_T)$ that an untreated virus has a value of the feature as low as x_T, which is the cumulative distribution function for the untreated sample: $P_I(x_T) = CDF_U(x_T)$. Thus, for the treated data points that are far away from the untreated events, the result would be zero while for the ones which has overlap, the result is more than zero. By assuming all untreated viruses are intact, we can consider a threshold, ε, on the probability P_I, and using a heaviside step function, θ, we decide if an event can be counted as an intact virus (if $P_I(x_T) \geqslant \varepsilon$) or not (if $P_I(x_T) < \varepsilon$). By applying this threshold on all events, we can define a function ρ_ε as equation 5 which is a sum on all treated data points normalized by the number of treated events, N.

$$\rho_\varepsilon = \sum_{i=1}^{N} \frac{\theta(P_I(x_i) - \varepsilon)}{N}. \quad (5)$$

So after treatment, there is $\rho_\varepsilon \times N$ number of events in the treated sample which have the probability larger than ε to be counted as the intact viruses. This count can be written as

$$\rho_\varepsilon \times N = n \times (1 - \varepsilon) + (N - n) \times q_\varepsilon, \quad (6)$$

where n in the first part is the actual number of intact viruses in the treated sample, and q_ε is the probability of counting a broken virus as an intact one in the treated sample. In this calculation, since $0 \leqslant q_\varepsilon \leqslant 1$, the r which is n/N, will be bounded by $r \leqslant \frac{\rho_\varepsilon}{1-\varepsilon}$. By minimizing the $\frac{\rho_\varepsilon}{1-\varepsilon}$ over the ε one can determine the upper bound for survival fraction. However there is another point to explore. This value of r has a large error bar due to the shot noise, so that the error in estimating n is proportional to the $\sqrt{n}$. In practice for large enough epsilon there will be no data points satisfying the condition of $P_I(x_T) \geqslant \varepsilon$ and the estimated value of ρ_ε would be zero. Thus as a practical approach, we consider a cutoff and vary epsilon from 0 to the maximal value at which $\rho_\varepsilon \times N \geqslant 5$, where 5 is an arbitrary threshold that controls how accurate this method is. As shown in figure 4(b) in our case, r_{max} can be estimated as 2.5×10^{-3} which is similar to the inverse of the reduction value $\sim 10^3$ reported using infectivity assays (figure 1(b)). So these data demonstrate that the proposed formulation makes it possible to determine the inactivation efficiency using the nanopore method; while in contrast to the conventional infectivity assays, the nanopore technique is capable of probing small damages to the viruses in linear base with high precision.

Generally the electrophoretic driving force and electroosmotic flow are the main effects that govern a particle's motion in a nanopore [43]. The first one originates from the force exerted to the charged nanoparticle in an electric field and the second one is due to the viscous drag by the fluid flowing through the charged nanopore in response to the applied voltage. Combining the equations for electrophoretic and electroosmotic transport yields an effective virus velocity v in an external electric field E inside the pore as [44]

$$v = \frac{E\varepsilon}{\eta}(\zeta_{virus} - \zeta_{pore}), \quad (7)$$

where ζ is zeta potential, η and ε are the viscosity and permittivity of the electrolyte. For our negatively charged viruses attempting to translocate through the nanopore with negative surface charge, these two forces oppose each other and the relative magnitudes of the forces determines the direction and duration of translocations [45].

In our study, electroosmotic flow is a dominant factor, and therefore, the difference in membrane and virus surface charge plays a dominant role on capture and transport. We were not able to observe a statistically significant difference between the zeta potential associated with treated and untreated virus samples. As shown in figure 3(e), the dwell time of most of the events in the treated sample are <90 μs, while untreated viruses have much longer dwell times. In addition, upon treatment, the dwell time distribution narrows substantially and the fractional current blockades are reduced, which can be attributed to a morphological change in the virus sample.

To further examine the impact of fs laser pulses on virus conformation, we employed DLS to characterize changes in the radius of ΦX174 viruses and its DNA caused by laser treatment. The DLS measured the average diameter of the untreated viruses 30.9 ± 2.3 nm (figure 5(a)), which is in agreement with the known ΦX174 particle size [46]. The DLS results demonstrate two useful pieces of information: first it shows that the laser-treated sample no longer possesses a monomodal size distribution and a second peak is observed at 458 ± 56 nm which will be discussed shortly. Another important piece of information can be obtained from the intersection of the correlation curve on the y-axis of the correlogram. This y-intercept is related to the signal-to-noise ratio of the measured sample. As shown in figure 5(b) the correlation coefficient for the treated ΦX174 viruses has a lower y-intercept of 0.4 compared to the untreated one which is ~0.85. The lower y-intercept in the treated sample can be attributed to the concentration variations in this sample and presence of 458 nm particles. This concentration variation can also be explored by nanopore measurements. In case of the nanopore measurements, the waiting time between two successive events (δt) is inversely proportional to the concentration of the detectable particles. An exponential fit to the waiting time data (figure 5(c)), indicates that capture rate of the viruses has decreased by more than one order of magnitude after laser treatment at the same voltage bias (40 mV). Capture rates for untreated and treated samples were 52 ± 0.87 s^{-1} and 3.49 ± 0.13 s^{-1} respectively.

Particles of the second mode in the DLS data of ΦX174 viruses have a hydrodynamic radius that is too large to be detected with our 38 nm nanopore. To investigate the second peak, we performed DLS measurement of ΦX174 virion DNA, the single-stranded viral DNA isolated from purified phage by phenol extraction (New England Biolabs). This measurement indicates if the second peak is a signature of free DNA ejected from virus under photonic exposure. The DLS measured average diameter of the untreated phenol-extracted DNA was 113.5 ± 30 nm. A part of this variation may be attributed to ~15% of the phenol-extracted DNA molecules not being in circular form. The radius of gyration, R_g and hydrodynamic radius, R_h of free ΦX174 DNA polymer can

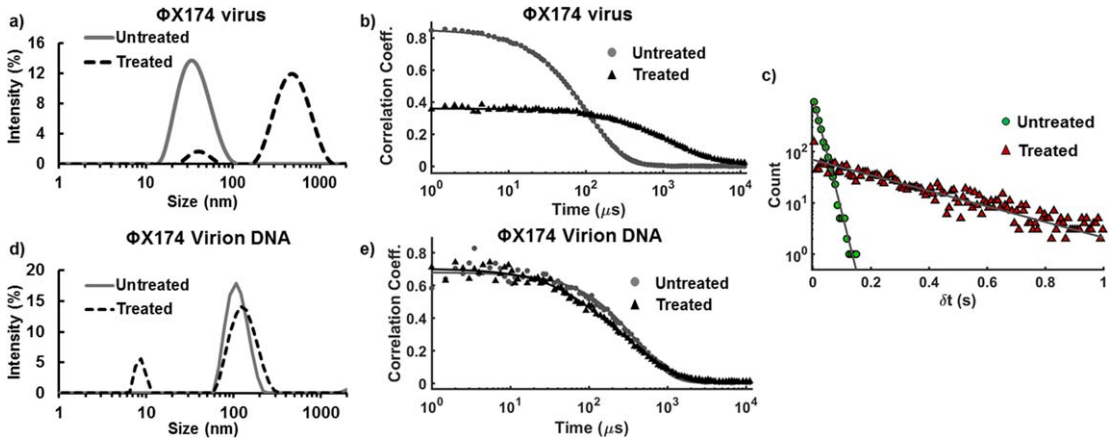

Figure 5. (a) DLS size distribution obtained from (b) quasi-elastic light scattering intensity autocorrelation function or correlogram of ΦX174 virus before (untreated) and after irradiation (treated) with IR& blue 35 fs laser pulses for 30 min (average laser power 2.5 W) (c) inter-event waiting time obtained from nanopore measurement of the data in figure 3 at 40 mV applied bias, fitted by an exponential function. (d) Size distribution (e) correlogram of ΦX174 viral DNA. Laser irradiation conditions were identical to (a), (b).

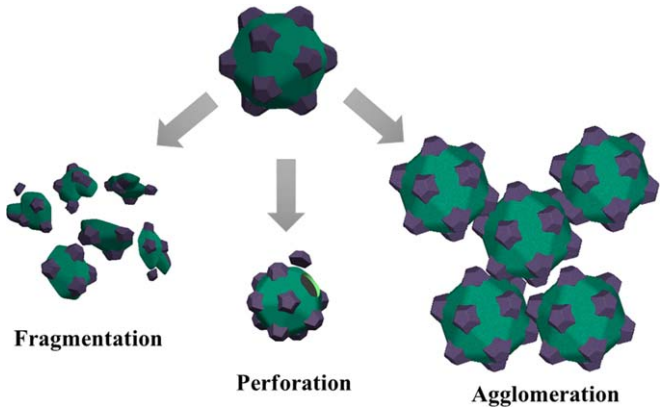

Figure 6. Schematic of the possible effect of the fs laser treatment on ΦX174 virus.

be estimated as

$$R_g = \sqrt{\frac{2PL_c}{6}}, \tag{8}$$

from the known persistence length P and the contour length L_c [47–49]. For ΦX174 DNA with 5386 nucleotides and the persistence length ~4.6 nm for DNA [50], the R_g and R_h can be estimated as 72 nm and 45.6 nm, respectively [41, 51]. So the corresponding hydrodynamic diameter is approximately 91 nm which is consistent with the peak in DLS measurement of untreated DNA. Interestingly, DLS data of laser exposed DNA (figure 5(d)), still contains this peak which argues against complete agglomeration of single-stranded DNA due to laser exposure. Also, as the correlogram of the DNA (figure 5(e)) shows there is little difference in the time autocorrelation function between exposed and unexposed DNA samples. Our observations indicate that the 458 nm peak observed in laser-treated ΦX174 viruses sample is thus not from the presence of free single-stranded DNA.

Based on our data after laser treatment there are three possible morphology changes that can happen to ΦX174 viruses: (i) fragmentation to small pieces, (ii) perforation of viruses that leads to DNA expulsion with a small associated change in the virus shell, and (iii) agglomeration of viral particles (figure 6). Nanopore data can be used to evaluate each of the possibilities. The fact that the fractional current blockade decreases after treatment, suggests that the particle diameter gets smaller upon laser exposure. Also if we neglect possible changes in the zeta potential of the viruses, the smaller viruses will translocate faster consistent with the observation of a shorter dwell times in the treated sample. Therefore, the current blockade and the dwell time both point to detection of entities smaller than the original viruses, and support the hypothesis of virus perforation. At the same time, the nanopore capture rate suggests that viruses for the most part have been fragmented to small pieces not detectable by the nanopore conductance.

Neither DLS nor nanopore data do not suggest extensive virus agglomeration. Since the differential scattering cross-section for elastic scattering in the Rayleigh regime is proportional to the 6th power of the particle radius with given dielectric properties, DLS may be expected to be sensitive to agglomeration or presence of larger particle species. Additionally, significant agglomeration is expected to lead to a higher intensity at second diffraction mode which is not observed. Also in the nanopore data, significant agglomeration of viruses can block the pore which leads to long lasting dwell times in contrast to what is observed in our experiments. So taken together, our data suggest that a small fraction of viruses (7%) get perforated, while a negligible fraction ($<10^{-3}$% based on Rayleigh scattering assumption) get agglomerated, and the remaining largest fraction of the viruses (93%) are fragmented.

While DLS provides an ensemble averaged estimate of the particle size distribution, it does not provide information at the single particle level. Our experiments suggest nanopore single-particle conductance measurements to be helpful in detecting intact viruses in small-volume samples (~0.5 μl) to characterize morphological changes caused by laser treatment and inactivation.

4. Conclusion

The ultrashort pulsed laser technology presented here can be readily used for rapid and effective disinfection of viruses in a label-free manner. Applying this technology to disinfect viruses can lead to some changes in the viruses which needs to be monitored with high precision. Nanopore technique allowed us to detect intact viruses and monitor the effect of fs laser on a model virus at the single virus level. Analysis of changes in the ionic current through the nanopore provides information about size and physical properties of viruses before and after laser treatment. To the best of our knowledge, this is the first time that nanopores have been used to monitor changes induced by an inactivation method in viruses.

Our data is a promising step towards developing a label-free detection technique that can also be used as an effective method for monitoring the survival fraction of viruses using low sample volume, high precision and fast assay time.

Acknowledgments

Grants: Kirill S Korolev was partially supported by Cottrell Scholar Award (#24010) by the Research Corporation for Science Advancement, a grant from the Simons Foundation (#409704) and an award from Gordon and Betty Moore foundation (#6790.08). X L and H Y were supported by the China Scholarship Council (CSC), and M A A was supported by the National Institutes of Health (R01-HG009186).

ORCID iDs

Shyamsunder Erramilli https://orcid.org/0000-0003-3950-9122

References

[1] AuBuchon J 2011 Update on the status of pathogen inactivation methods *ISBT Sci. Ser.* **6** 181–8
[2] Hellstern P 2004 Solvent/detergent-treated plasma: composition, efficacy, and safety *Curr. Opin. Hematology* **11** 346–50
[3] Rock G 2011 A comparison of methods of pathogen inactivation of FFP *Vox Sanguinis* **100** 169–78
[4] Nazari M, Xi M, Lerch S, Alizadeh M, Ettinger C, Akiyama H, Gillespie C, Gummuluru S, Erramilli S and Reinhard B M 2017 Plasmonic enhancement of selective photonic virus inactivation *Sci. Rep.* **7** 11951
[5] Tsen K-T, Tsen S-W D, Chang C-L, Hung C-F, Wu T-C and Kiang J G 2007 Inactivation of viruses by laser-driven coherent excitations via impulsive stimulated Raman scattering process *J. Biomed. Opt.* **12** 064030–6
[6] Tsen K T, Tsen S-W D, Fu Q, Lindsay S M, Li Z, Cope S, Vaiana S and Kiang J G 2011 Studies of inactivation of encephalomyocarditis virus, M13 bacteriophage, and Salmonella typhimurium by using a visible femtosecond laser: insight into the possible inactivation mechanisms *J. Biomed. Opt.* **16** 078003–8
[7] Tsen S-W D, Chapa T, Beatty W, Tsen K-T, Yu D and Achilefu S 2012 Inactivation of enveloped virus by laser-driven protein aggregation *J. Biomed. Opt.* **17** 128002
[8] Tsen S-W D, Kingsley D H, Poweleit C, Achilefu S, Soroka D S, Wu T and Tsen K-T 2014 Studies of inactivation mechanism of non-enveloped icosahedral virus by a visible ultrashort pulsed laser *Virology J.* **11** 20
[9] Tsen K, Tsen S-W D, Hung C-F, Wu T and Kiang J G 2008 Selective inactivation of human immunodeficiency virus with subpicosecond near-infrared laser pulses *J. Phys.: Condens. Matter* **20** 252205
[10] Tsen S-W D, Tsen Y-S D, Tsen K and Wu T 2010 Selective inactivation of viruses with femtosecond laser pulses and its potential use for *in vitro* therapy *J. Healthc. Eng.* **1** 185–96
[11] Kangro H O and Mahy B W 1996 *Virology Methods Manual* (New York: Academic)
[12] Daaboul G, Yurt A, Zhang X, Hwang G, Goldberg B and Unlu M 2010 High-throughput detection and sizing of individual low-index nanoparticles and viruses for pathogen identification *Nano Lett.* **10** 4727–31

[13] Mitra A, Deutsch B, Ignatovich F, Dykes C and Novotny L 2010 Nano-optofluidic detection of single viruses and nanoparticles *ACS Nano* **4** 1305–12
[14] Stoffel C L, Kathy R F and Rowlen K L 2005 Design and characterization of a compact dual channel virus counter *Cytometry* A **65** 140–7
[15] Harms Z D, Haywood D G, Kneller A R, Selzer L, Zlotnick A and Jacobson S C 2014 Single-particle electrophoresis in nanochannels *Anal. Chem.* **87** 699–705
[16] Piruska A, Gong M, Sweedler J V and Bohn P W 2010 Nanofluidics in chemical analysis *Chem. Soc. Rev.* **39** 1060–72
[17] Cressiot B, Oukhaled A, Patriarche G, Pastoriza-Gallego M, Betton J-M, Auvray L C, Muthukumar M, Bacri L and Pelta J 2012 Protein transport through a narrow solid-state nanopore at high voltage: experiments and theory *ACS Nano* **6** 6236–43
[18] Freedman K J, Haq S R, Edel J B, Jemth P and Kim M J 2013 Single molecule unfolding and stretching of protein domains inside a solid-state nanopore by electric field *Sci. Rep.* **3** 1638
[19] Freedman K J, Jürgens M, Prabhu A, Ahn C W, Jemth P, Edel J B and Kim M J 2011 Chemical, thermal, and electric field induced unfolding of single protein molecules studied using nanopores *Anal. Chem.* **83** 5137–44
[20] Ledden B, Fologea D, Talaga D S and Li J 2011 *Nanopores* (Berlin: Springer) pp 129–50
[21] Li J, Fologea D, Rollings R and Ledden B 2014 Characterization of protein unfolding with solid-state nanopores *Protein Peptide Lett.* **21** 256–65
[22] Oukhaled A, Cressiot B, Bacri L, Pastoriza-Gallego M, Betton J-M, Bourhis E, Jede R, Gierak J, Auvray L C and Pelta J 2011 Dynamics of completely unfolded and native proteins through solid-state nanopores as a function of electric driving force *ACS Nano* **5** 3628–38
[23] Talaga D S and Li J 2009 Single-molecule protein unfolding in solid state nanopores *J. Am. Chem. Soc.* **131** 9287–97
[24] Alibakhshi M A, Halman J R, Wilson J, Aksimentiev A, Afonin K A and Wanunu M 2017 Picomolar fingerprinting of nucleic acid nanoparticles using solid-state nanopores *ACS Nano* **11** 9701–10
[25] Branton D, Deamer D W, Marziali A, Bayley H, Benner S A, Butler T, Di Ventra M, Garaj S, Hibbs A and Huang X 2008 The potential and challenges of nanopore sequencing *Nat. Biotechnol.* **26** 1146–53
[26] Carson S and Wanunu M 2015 Challenges in DNA motion control and sequence readout using nanopore devices *Nanotechnology* **26** 074004
[27] Braha O, Gu L-Q, Zhou L, Lu X, Cheley S and Bayley H 2000 Simultaneous stochastic sensing of divalent metal ions *Nat. Biotechnol.* **18** 1005–7
[28] Movileanu L, Cheley S and Bayley H 2003 Partitioning of individual flexible polymers into a nanoscopic protein pore *Biophys. J.* **85** 897–910
[29] Zhou K, Li L, Tan Z, Zlotnick A and Jacobson S C 2011 Characterization of hepatitis B virus capsids by resistive-pulse sensing *J. Am. Chem. Soc.* **133** 1618–21
[30] Harms Z D, Mogensen K B, Nunes P S, Zhou K, Hildenbrand B W, Mitra I, Tan Z, Zlotnick A, Kutter J P and Jacobson S C 2011 Nanofluidic devices with two pores in series for resistive-pulse sensing of single virus capsids *Anal. Chem.* **83** 9573–8
[31] Arjmandi N, Van Roy W and Lagae L 2014 Measuring mass of nanoparticles and viruses in liquids with nanometer-scale pores *Anal. Chem.* **86** 4637–41
[32] Arjmandi N, Van Roy W, Lagae L and Borghs G 2012 Measuring the electric charge and zeta potential of nanometer-sized objects using pyramidal-shaped nanopores *Anal. Chem.* **84** 8490–6
[33] Wu H, Chen Y, Zhou Q, Wang R, Xia B, Ma D, Luo K and Liu Q 2016 Translocation of rigid rod-shaped virus through various solid-state nanopores *Anal. Chem.* **88** 2502–10
[34] Tsen K-T, Tsen S-W D, Fu Q, Lindsay S M, Kibler K, Jacobs B, Wu T C, Karanam B, Jagu S and Roden R B 2009 Photonic approach to the selective inactivation of viruses with a near-infrared subpicosecond fiber laser *J. Biomed. Opt.* **14** 064042–7
[35] Thompson S S and Yates M V 1999 Bacteriophage inactivation at the air-water-solid interface in dynamic batch systems *Appl. Environ. Microbiol.* **65** 1186–90
[36] Liu X, Dai Q, Austin L, Coutts J, Knowles G, Zou J, Chen H and Huo Q 2008 A one-step homogeneous immunoassay for cancer biomarker detection using gold nanoparticle probes coupled with dynamic light scattering *J. Am. Chem. Soc.* **130** 2780–2
[37] Tsen K-T, Tsen S-W D, Chang C-L, Hung C-F, Wu T and Kiang J G 2007 Inactivation of viruses by coherent excitations with a low power visible femtosecond laser *Virology J.* **4** 50
[38] Tsen S-W D, Wu T C, Kiang J G and Tsen K-T 2012 Prospects for a novel ultrashort pulsed laser technology for pathogen inactivation *J. Biomed. Sci.* **19** 62
[39] Brough H, Antoniou C, Carter J, Jakubik J, Xu Y and Lutz H 2002 Performance of a novel viresolve NFR virus filter *Biotechnol. Prog.* **18** 782–95
[40] Kim M J, Wanunu M, Bell D C and Meller A 2006 Rapid fabrication of uniformly sized nanopores and nanopore arrays for parallel DNA analysis *Adv. Mater.* **18** 3149–53
[41] Waduge P, Hu R, Bandarkar P, Yamazaki H, Cressiot B, Zhao Q, Whitford P C and Wanunu M 2017 Nanopore-based measurements of protein size, fluctuations, and conformational changes *ACS Nano* **11** 5706–16
[42] Larkin J, Henley R Y, Muthukumar M, Rosenstein J K and Wanunu M 2014 High-bandwidth protein analysis using solid-state nanopores *Biophys. J.* **106** 696–704
[43] Huang G, Willems K, Soskine M, Wloka C and Maglia G 2017 Electro-osmotic capture and ionic discrimination of peptide and protein biomarkers with FraC nanopores *Nat. Commun.* **8** 935
[44] Firnkes M, Pedone D, Knezevic J, Döblinger M and Rant U 2010 Electrically facilitated translocations of proteins through silicon nitride nanopores: conjoint and competitive action of diffusion, electrophoresis, and electroosmosis *Nano Lett.* **10** 2162–21627
[45] Melnikov D V, Hulings Z K and Gracheva M E 2017 Electro-osmotic flow through nanopores in thin and ultrathin membranes *Phys. Rev.* E **95** 063105
[46] Bayer M and DeBlois R 1974 Diffusion constant and dimension of bacteriophage ΦX174 as determined by self-beat laser light spectroscopy and electron microscopy *J. Virology* **14** 975–80
[47] Boal D and Boal D H 2012 *Mechanics of the Cell* (Cambridge: Cambridge University Press)
[48] Rechendorff K, Witz G, Adamcik J and Dietler G 2009 Persistence length and scaling properties of single-stranded DNA adsorbed on modified graphite *J. Chem. Phys.* **131** 09B604
[49] Sim A Y, Lipfert J, Herschlag D and Doniach S 2012 Salt dependence of the radius of gyration and flexibility of single-stranded DNA in solution probed by small-angle x-ray scattering *Phys. Rev.* E **86** 021901
[50] Manning G S 2006 The persistence length of DNA is reached from the persistence length of its null isomer through an internal electrostatic stretching force *Biophys. J.* **91** 3607–16
[51] Tree D R, Muralidhar A, Doyle P S and Dorfman K D 2013 Is DNA a good model polymer? *Macromolecules* **46** 8369–82